5

Advanced AE Technology for High-Power Microwave Radar Tubes

Narayan R. Joshi, Stephen D. Russell,
Ayax D. Ramirez and David W. Brock
HCC-NW, Houston, Texas and SPAWARSYSCEN PACIFIC, San Diego, California, USA

1. Introduction

Acoustic emission (AE) and micro-seismic activity are naturally occurring phenomena. Almost all materials emit sound or acoustic emission when they are sufficiently stressed. Wood and rock produce AE signals in audible frequency ranges when stressed. It was also believed that AE signal generation could exist in the ultrasonic frequency range during deformation of materials, but it was not until 1950 when Joseph Kaiser reported the first comprehensive investigations on acoustic emission phenomenon in conventional engineering materials using electronic equipment and tensile testing machines. Kaiser also observed that AE activity was irreversible. Acoustic emissions are not generated during the reloading of a material until the stress level has exceeded its previous highest value. This AE irreversible phenomenon is now known as the Kaiser Effect. He also proposed a distinction between burst and continuous AE activity. The use of piezoelectric sensors and electronic amplifiers to observe high-frequency AE activity gradually led to the definition of acoustic emission. According to the ASNT Handbook (1987), acoustic emission refers to the generation of transient elastic stress (strain) waves due to the rapid release of energy from a localized source within a material undergoing some kind of deformation. The kind of stress applied to materials under testing could be tensile, compressive or shear. The transient elastic stress waves of AE have frequencies ranging from 20 kHz (kilohertz) to 1 MHz (megahertz). Green (1980) has listed many mechanisms that produce acoustic emission activity in materials. Among them, the principal mechanisms are mechanical deformation, fracture, crack propagation, dislocation motion and multiplication, twin formation, phase transformation, corrosion, friction and internal magnetic processes. Mechanical loading is not the only way to generate AE activity (phonon signals). Thermal shock loading and electrical sparking are also known to cause AE activity. Generation of AE activity during chemical reactions has also been observed. It was realized quite earlier that AE activity appears in two types, burst signals and continuous signals.

2. Acoustic emission as a nondestructive evaluation technique

Applications of acoustic emission technology are growing rapidly with the improvement of AE instrumentation through several generations of refinement. It has reached a stage in which it is now used as a reliable nondestructive testing technique (NDT) in industry along

with conventional techniques of ultrasonics, magnetic particles testing, liquid penetrants testing and eddy current testing. In certain industrial applications in which performance monitoring of systems occurs around the clock, acoustic emission is the only alternative available. Currently, acoustic emission testing offers high level of performance and user convenience. Although most of AE research and development took place in metallurgy and materials science in the early years, its usefulness was soon observed in many fields beyond metallurgical applications.

AE signals cover a wide range of energy levels and frequencies, from several hertz up to tens of megahertz, with two basic types of signals generally observed—burst and continuous. Some stimulus is necessary to trigger acoustic emissions. Stress, a major type of stimuli, may be mechanically applied, thermally generated, or caused by a changing magnetic field. AE sensors (transducers) convert stress wave parameters of the source event into electrical voltages corresponding to the detected event. The most popular sensor for acoustic emission experiments is a piezoelectric ceramic element, which produces a detectable response to a quick displacement change of 10^{-12} inch. The amplification of the detected signal is usually conducted in two steps to attain gains of up to 120 dB (decibels). The signals are also passed through appropriate filters for elimination of a large part of the background noise. Depending on the application, the subsequent signal may be analyzed either in the time domain or in the frequency domain. For many applications requiring frequency analysis in the range of 0.1 to 2 MHz, a broadband transducer is used. However, such transducers have a lower signal-to-noise ratio when compared with the resonant narrow-band transducers.

The propagation medium which causes attenuation, reflections and mode conversions, greatly affects the frequency content, which is also affected by the transducer and electronic system used in the experiment. Often, it is impossible to measure quantitatively the magnitude of the source of the AE signal. However, AE activity from an undamaged structure differs from the one undergoing damage over time. The relative changes in AE activity can be used to estimate changes in structural integrity of the system. From this point of view, AE technique has established itself as one of the advanced NDT (nondestructive testing) techniques in different engineering fields.

3. Applications of acoustic emission to electromagnetics

Recently, acoustic emission was used to detect electrical arcing from a sputtering target. The conventional arc detection technique involves the detection of voltage or current spikes occurring in the power supply line when the arc is initiated. This technique is not immune to unwanted electrical noise signals and may generate a false count. Therefore, the implementation of the nonelectric arc detection and counting technique may provide some advantage by improving noise immunity. Leybovich and Ferdinand (2001) used an arc detection and counting technique that monitors the acoustic emission signals generated by the arcing event**.** They observed that the AE response of the genuine arc generates a relatively long ringing radio frequency (RF) pulse with a significant number of cycles exceeding the threshold level. The prolonged cycling makes it possible to differentiate true arcing from false indications. The fundamental principle of this method is based on the phenomenon of generating an acoustic pulse when the arc generated shock wave strikes a solid. Sakoda and Nieda (2001) measured the characteristics of AE signals generated by a

single pulse corona discharge and used them as a diagnostic tool to estimate insulation deterioration in oil immersed pole transformers. Boczar (1999 and 2001) used frequency analysis of AE signals generated by partial discharges to distinguish them from AE signals generated by corona discharges. Vahaviolos and Monsoor (1976) observed acoustic emission during laser spot welding. When the laser beam is absorbed by the surface of the material during welding, thermal stresses are generated leading to a stress wave packet due to the elastic behavior of the material. Tsukamoto and Iwasa (1986) used acoustic emission as a diagnostic and monitoring technique for arcing in a superconducting magnet. Commercial nondestructive testing companies are using acoustic emission technology to test power transformers for partial discharge, hot spots, arcing, loose connections and core clamping problems.

4. Problems with high-power microwave radar tubes

Microwave tubes used in high-power radar and communications systems are expensive. They have an operating life of a few thousand hours. When an expensive tube fails, it is generally impossible to determine the sequence of events that contributed to its failure. Three types of transmitting devices have been dominant in radar for many years. They are the magnetron, the klystron and the traveling wave tube. All are based on vacuum-tube technology. They are high vacuum devices (10^{-7} to 10^{-8} Torr). Their electrode voltages can run in excess of 10 kV (kilovolts). High heat dissipation (100 W (watts) to 10 kW (kilowatts)) is involved. Currently, microprocessor-based systems with as many as 11 sensors are designed to monitor tube performance, provide tube protection and record a comprehensive tube failure history. Watson and Troy (1987) discussed major limitations with these systems that results from the small amount of time available during the inter-pulse period of the tube for data buffering and fault analysis. The current monitoring systems work well if the microwave tube is operated at 200 pulses per second or less. However, most radar tubes are operated at up to 1000 pulses per second with pulse duration of a microsecond. Increasing data acquisition speed will, in some case, make the situation worse, since it will increase the amount of data that must be transferred and analyzed during the limited time interval available.

5. Acoustic emission as in-situ performance monitoring technique

Existing performance monitoring systems do not satisfy the modern requirements of NDT of high-power microwave tubes. Sensors that are self-contained, that could be battery powered or integrated with wireless telemetry are preferable. They should be nonintrusive and electrically isolated. They are expected to be inexpensive and compact. Two NDT techniques considered for microwave tubes included ultrasonics and acoustic emission. Ultrasonics is an active technique where high-frequency sound waves or pulses are injected into a test object and then echoes of the incident signal are monitored. Since the microwave tubes are high-power electronic devices, an active technique like ultrasonics may interfere with tube operation. On the other hand, AE is a passive technique where elastic stress waves of high frequencies generated by a device in operation can be monitored safely and externally without interfering with the normal operation of the radar tubes. The concept behind the in-situ performance monitoring of a high-power radar tube is as follows: Every time the tube generates a high–power radio-frequency pulse, it also produces a shock pulse in the tube body. An acoustic emission sensor coupled to the tube body then detects the

pulse. As the tube ages, it starts to occasionally malfunctioning during pulse generation usually due to arcing, generating abnormal AE signals. Its progressive aging is characterized by monitoring of the increasingly abnormal AE signals. This technique enables decision-making to determine whether to determine whether to keep the tube in operation only a few more months or for several more years. In short, recording of AE activity is like listening to the tube, which in turn, provides an elegant, simple and inexpensive NDT tool for in-situ performance monitoring of high power microwave radar tubes.

The fundamental principle of this method is based on the phenomenon of the generation of an acoustic pulse when the arc-generated shock wave strikes a solid. In a recent experiment, characteristics of AE signals generated due to a single pulse corona discharge were measured and used as a diagnostic tool to estimate insulation deterioration in oil-immersed pole transformers. Frequency analysis of AE signals generated by partial discharges was used to distinguish them from AE signals generated by corona discharges.

Theobald et al. (2001) pointed out the difference between the AE event energy (AE_{energy}) and the AE energy descriptor (E_{AE}). The AE event energy (AE_{energy}) is given by

$$AE_{energy} \propto \int_0^T V(t)$$

Generally, AE stress waves disperse throughout the medium until interaction with an interface or boundary leads to the production of a reverberating field. Although this energy will be mostly absorbed by the medium, some of the energy can be detected by the use of a high-frequency piezoelectric ceramic transducer. Assuming all mechanisms of energy loss in the structure and measurement system are constant, then the measured electrical signal energy from the transducer could be said to be proportional to the AE event energy (AE_{energy}). Here T is the time length of transient signal produced and V(t) is the transient voltage. The measured electrical signal energy is often referred to as the AE energy descriptor (E_{AE}) and is written as

$$E_{AE} \propto \left(\frac{1}{R}\right)\int_0^T V(t)^2 dt \ ,$$

where E_{AE} refers to the AE energy measured in the transducer and R is the impedance of the complete measuring circuit. The power of the acoustic emission signal of the detected event is thus proportional to the power of the source event. The advantage of energy measurement over ring down counting is that energy measurements can be directly related to important physical parameters without having to model the acoustic emission signal. Energy measurements also improve the acoustic emission measurement when emission signal amplitudes are low.

6. Acoustic emission equipment

A new AE technique was developed, for performance monitoring purposes, to detect and measure the AE activity of radar tubes in operation. This section describes the equipment used for such a technique and some calibration procedures. Subsequent sections describe the methodology employed.

6.1 Acoustic emission transducers

Four transducers are used in this study. They are A, B, and C bought from a well-known commercial company located in the USA and D from a second company. A truncated conical aluminum piece is prepared as a match between the curved surface of the anode of the magnetron and the flat front surface of the sensors. The A sensor has peaks at 100, 300 and 500 kHz. The B sensor shows peak responses at frequencies 130, 300 and 390 kHz according to data from the manufacturer. The C sensor is highly damped with tungsten powder backing. The fourth sensor, D, was a broadband sensor. The characteristics of the four transducers or sensors were independently determined in this work and they corresponded to those supplied by their manufacturer.

These AE transducers are physically coupled to the device under test using a viscous or gel-type coupling compound.

Transducer	Description
A	General purpose transducer for monitoring acoustic emission (AE) activity in the range of 100 to 700 kHz
B	General purpose transducer for monitoring acoustic emission (AE) activity in the range of 200kHz to 1MHz
C	Wideband displacement sensor with flat response over the frequency range of 20 kHz to 1 MHz
D	Broadband sensor with flat response over the frequency range of 1 kHz to1.5 MHz

Table 1. Transducers chosen for research.

6.2 Acoustic Emission pre-amplifier

The 2/4/6 preamplifier used in this work has three gain settings of 20, 40, and 60 dB with a high-input impedance (greater than 20 MΩ (megohms). It can produce a large output signal up to 20 V (volts) peak to peak in 50 Ω (ohms). The useful frequency range of the preamplifier used in this work is 100 kHz to 1 MHz.

6.3 Acoustic Emission post-amplifier

The Model AE1A was used as the post-amplifier. The total gain achievable in 3-dB steps is 41 dB. The input impedance at the terminal "AE INPUT" is 50 ohms and at the terminal "AE OUT" is 50 ohms. The useful frequency range as tested in this work is 100 kHz to 1 MHz. The pre-amplifier receives about 21 volts DC from the post- amplifier on the same cable that carries the AE signal from the preamplifier to the postamplifier.

6.4 The oscilloscope

The oscilloscope used to monitor AE activity was a LeCroy Model 9354AM. Each of the oscilloscope's four input channels is equipped with a 500 MS/s (million samples per second), 8 bit A/D converter. Acquisition memories of up to 2 million points simplify transient capture by providing long waveform records that capture waveforms even when trigger timing or signal speed is uncertain. The important feature of the oscilloscope is its

500-MHz bandwidth. The data from the screen can be dumped and stored on a 3.5-inch floppy disk. This completes the description of the equipment setup.

6.5 Calibration of transducers

The literature provides a standardization method for calibrating AE sensors by using a capacitive transducer to capture the initial arrival of a displacement signal produced by the fracture of a glass capillary. This procedure allowed the development of quantitative comparison of AE experiment with theories of the wave propagation. AE activity may be of discrete or continuous nature. Attempts were made to generate standard pulses, which for discrete ones, correspond to the delta function, whereas in case of continuous emission, to white noise. The standard signal should be characterized by parameters determined in time and frequency domains as close to the AE signal source as possible. In the current work, it was decided to use the mechanical pencil lead breaking procedure to simulate an AE source of discrete nature. This procedure was performed on a circular aluminum plate a half-inch thick and six inches in diameter. The lead was broken on the plate at a distance of one half-inch from the AE transducer coupled with silicone grease to the same surface of the plate. AE signals were monitored on the oscilloscope. All four transducer showed satisfactory results.

7. Application of AE technology to high power microwave tube magnetron

The high-power microwave tube used in this experiment was a magnetron (Model 2J55). The magnetron oscillator is small, lightweight, operates at reasonable voltages, and has good efficiency, rugged construction and long life. The magnetron was the first practical high-power pulsed radar source used at microwave frequencies, and it is still rather widely used today. The magnetron converts energy extracted from a pulsed electric current to RF energy. The magnetron consists essentially of a copper ring into which resonant cavities have been machined. These cavities connect with the center of the ring via slots. A cathode is mounted at the center of the rings and an axial magnetic field is applied to the whole system by permanent magnets. The application of a high voltage to the ring anode with respect to cathode results in the emission of electrons from the cathode. Thus, electric field E and magnetic field H are crossed in the interaction region. Hence, magnetron is called a crossed-field device. In traveling towards the anode, paths of electrons are curved by the longitudinal magnetic field, and their trajectory takes them past the slots cut in the outer ring. If the conditions are chosen correctly, the electrons will give up some kinetic energy as they pass the slots. The energy given up will increase the amplitude of the oscillations in the cavity.

When the magnetron is oscillating, the cavities are coupled together by oscillatory E and H fields and energy is therefore extracted from all cavities by a loop within a single cavity. In an 8-cavity magnetron, these cavities form four spokes centered on the cathode**.** The magnetron is a kind of diode and Figure 1(a) shows its simplified schematic. A cutaway view of one possible magnetron configuration is shown in Figure 1(b) after T. C. Edwards (1984). The principal parts of magnetron are the cathode, the interaction region, the cavities, and the output coupling. The voltage/current relationship for a microwave magnetron is nonlinear and hence the magnetron is often represented by an equivalent circuit consisting of a biased diode with the magnetron's stray capacitance represented by a capacitor connected in parallel. An appreciable current is not drawn by a conventional magnetron until a critical voltage, approximately 90% of the operating voltage is reached. This voltage

is called Hartree voltage. Low levels of RF output power may be generated by the tube even below the Hartree voltage. Therefore, care should be taken to ensure that voltage is promptly removed after the desired pulse and not reapplied, even at low levels.

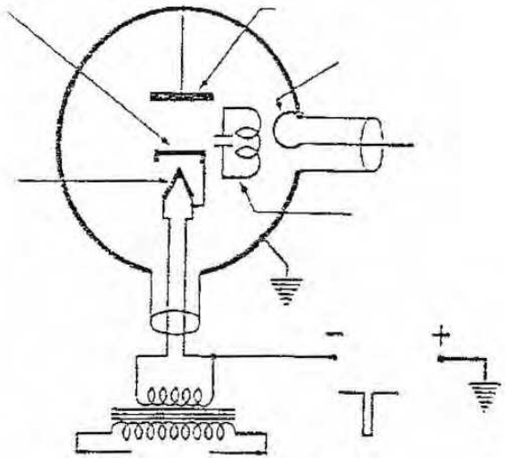

Fig. 1.(a) Simple schematic of Magnetron Tube.

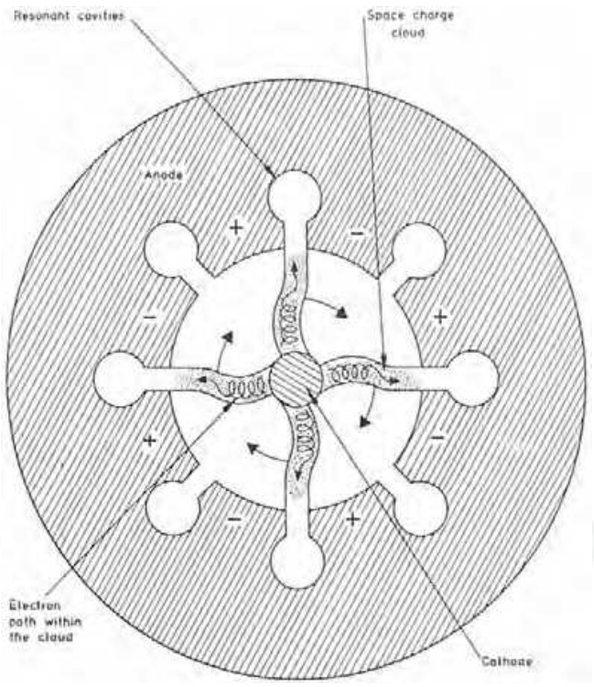

Fig. 1.(b) Electron paths in Magnetron

7.1 Magnetron operating characteristics

When a voltage pulse of the proper magnitude (-15 kilovolt DC) and a magnetic field of the correct strength (1900 to 2100 gausses) are applied, the magnetron will oscillate at a frequency determined by the magnetron cavity which acts like a tuned circuit. The RF (radio frequency) generated by the magnetron used in this work was 9.4 GHz (gigahertz). The size

of the cavities may be around 2 mm. The cavity is coupled inductively to a pick-up loop which is connected to the inner conductor of a waveguide. Thus, the output of the magnetron was connected to a waveguide terminated in a load cooled by fins and air blower. The peak input power to the magnetron was 210 kW and the peak output power was 50 kW. The average current drawn by the magnetron is about 1.2 mA (milliampere) but the current during 1-μs (microsecond) pulse is about 20 A (amperes). The duty cycle (width of pulse/period between pulse = 1 μs/0.01666 s) for 60 pulses per second is 0.006 percent.

One problem with magnetron oscillators is that the interaction space in a magnetron will support more than one possible mode of oscillation. In well-designed magnetrons, the various modes are well separated in both voltage and frequency and the magnetron will operate in the desired mode in a stable manner. However, certain parameters, notably the characteristics of the modulator, such as the rate of rise of voltage, can strongly influence the mode selection in magnetrons. Operation in other than the normal mode (called moding) is usually undesirable, because oscillations are separated from the normal operating frequency and the power does not couple out of the tube in the proper fashion. Double moding can be detected by the appearance of a smaller pulse, which varies in amplitude underneath the main pulse. Double moding could happen due to a change in loading, in magnetic field strength, or in applied voltage.

Another property of magnetrons, which is probably related to moding, is the tendency of such tubes to produce an occasional RF output pulse of reduced amplitude or to fail to produce any RF output pulse. In a well-designed tube, such missing pulses would typically occur less often than 1 in 10^4. As with any high-power tube, the possibility of internal tube arcing always exists. Particularly in case of magnetrons, internal arcing is one factor that must be given attention in the design of the modulator or pulser to drive the tube. The outside of the magnetron is a grounded shell to which the plate of the magnetron is connected (Figure 1(a)). The cathode has a negative potential with respect to the anode. The cathode of the tube is heated indirectly and connected to one side of the filament. The filament is fed by the transformer, which is highly insulated to withstand the peak modulator pulse voltage applied to the cathode. The high-voltage pulse is applied to the magnetron through a high-voltage concentric bushing.

The output frequency varies about 0.05 MHz per degree change in magnetron temperature. Thus, a gradual frequency shift may be observed during initial warm-up period. An air blower cools the magnetron during normal operation and a temperature sensor connected to a digital readout device monitors the temperature. As mentioned before, the resistance of the magnetron is nonlinear. At low plate voltage values, changes of large plate voltage result in minor changes in plate current. In the normal operating mode, however, a 10% increase in plate voltage may produce a 100% increase in plate current, depending on the characteristics of the tube under use at a given value of the magnetic field strength. A decrease in magnetic flux density with constant plate voltage causes a large increase in plate current. A good operating procedure requires decrease in plate voltage to go with decrease in flux density and no operation of magnetron without a magnetic field.

7.2 Waveguides and VSWR

A waveguide can be used to minimize losses and produce high-power transmission at microwave frequencies. It consists of a single metallic conductor in the shape of rectangular

box or cylinder, through which the electromagnetic waves are propagated. Such guided waves have field configurations somewhat different from those of two wire open lines. The waveguide transmission is characterized by two important features. First, below a minimum frequency a given waveguide will not transmit the wave. This is called the cut-off frequency, f_c, and is directly related to the size of the waveguide used. Second, a component of E or H always exists along the direction of propagation. The guided waves may be propagated along the waveguide with different field patterns called 'modes.' Modes are mainly of two types: those that have an E component along the direction of propagation are called TM or E waves, and those with an H component along the direction of propagation, which are called TE or H waves. Rectangular waveguides have losses less than those of circular waveguides and are less prone to mode changing. Hence, they are commonly used. The magnetron in the current work was also connected to a rectangular waveguide. Waveguides are usually made of brass, copper, or aluminum in various standard sizes corresponding to microwave frequencies used. Waveguide sections are usually coupled together by flanged assemblies that are bolted together and supported periodically on metal stands. The parameters associated with the rectangular or circular waveguide are impedance Z and cutoff wavelength λ_c, and they are closely related to dimensions of the waveguide, while attenuation losses depend on these factors as well as on the inner surface finish and metal of the waveguide walls. Just to give an example, some figures for the TE_{10} wave mode in rectangular waveguide are given next,

$$Z_{TE}\,(\text{Ohms}) = 377\lambda_g / \lambda \text{ and } \lambda_c = 2a,$$

where λ_g is the guide wavelength, λ is the free space wavelength, λ_c is the cutoff wavelength, and a is the width of the waveguide. See Connor (1972).

The magnetron can be attached to a waveguide to inject microwaves into it where they will propagate as a sinusoidal wave. If the load absorbs all of the wave, then there is no reflection. This occurs when the resistive load and the source load have equal impedance. This condition is called a matched load. But if there is a mismatch, then not all of the incident power is absorbed by a load and some of it is reflected back. The reflected wave then combines with the transmitted wave, resulting in standing wave. The ratio of the maximum and minimum amplitudes is called the voltage standing wave ratio or VSWR. It is important that the VSWR of the load is known, because if a VSWR is too high, an appreciable amount of energy will be reflected back to magnetron, which could cause severe damage. The VSWR can be written as

$$\text{VSWR} = V_{max} / V_{min} = (Vi + Vr) / (Vi - Vr),$$

where Vi and Vr are the voltage due to the incident and reflective wave, respectively. The VSWR can be measured with a network analyzer or with the slotted line method using a probe and VSWR meter**.** See Love (1995).

7.3 Experimental setup

Figure 2 shows the schematic of the experimental apparatus. The photo of the actual magnetron unit is presented in the report of Joshi et al. (2000). The AE signal is fed to one channel of the LeCroy digital oscilloscope. The cathode current pulse is fed to the second channel. The cathode voltage through a high-voltage probe (Tektronix, Model 015-049) is connected to the third channel. The high-voltage pulses have negative polarity since they

are fed to the cathode while the anode is grounded. In Figure 2, an Interstate P25 Pulse generator is shown under the oscilloscope. Its pulsed output goes to the external trigger on the oscilloscope and to the pulser trigger on the left-hand cabinet of the modulator for the magnetron. The oscilloscope displays four (processed) traces A, B, C, and D and is capable of mathematical analysis and zooming of each trace. The scope had the capacity to test a waveform against a predefined mask, which made it possible to catch on the screen abnormal current pulses and run mathematical operations such as FFT (Fast Fourier Transform) of AE signals, which could help show abnormal functioning of the magnetron.

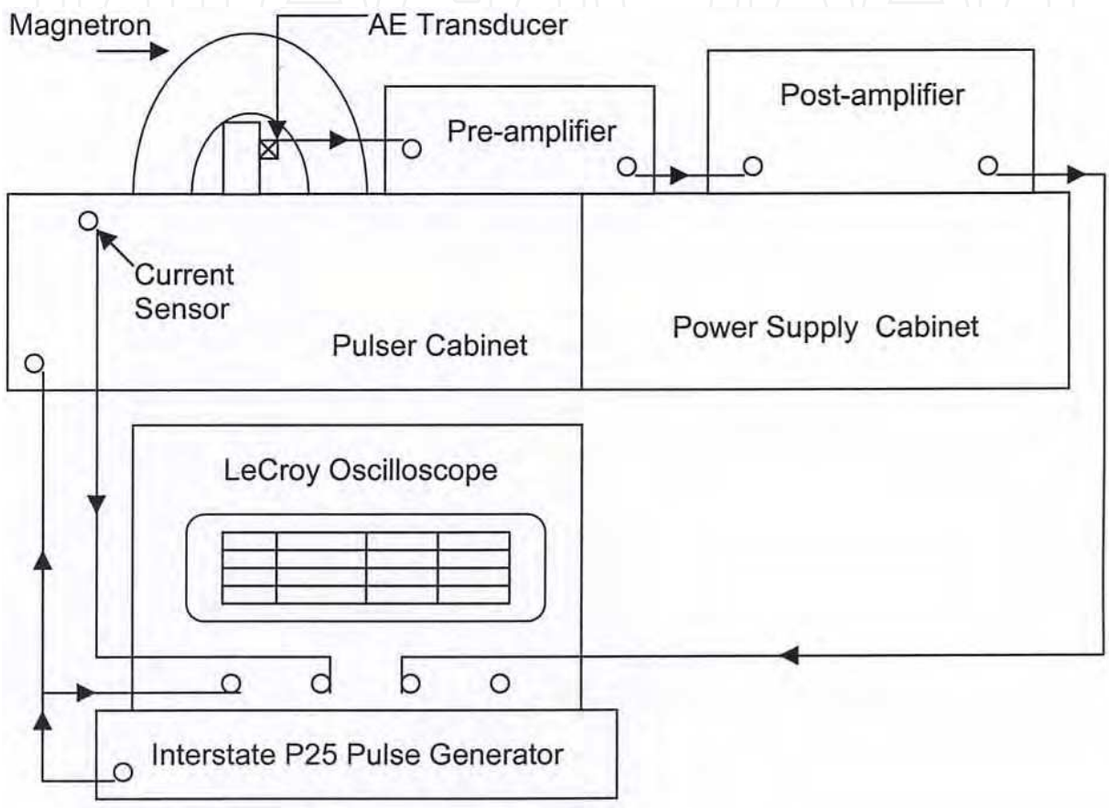

Fig. 2. Schematic of Experimental Equipment.

The magnetron was purposely stressed by changing parameters from their normal values prescribed for stable operation. This allowed accelerated aging and generated abnormal cathode current pulses leading to abnormal RF pulses. The magnitude of the FFT of the AE activity picked up during abnormal functioning of the tube was computed and all traces from the screen were saved to the disk. These traces were compared with those obtained during the stable or normal functioning of the tube. This testing procedure showed whether the acoustic emissions generated by the pulsating magnetron could be used as a noninvasive method for monitoring the normal and abnormal functioning of the tube.

7.4 Experimental procedure

The proper operation of the magnetron depends on the amplitude of the voltage pulse applied, the strength of the magnetic field, and the proper loading of the magnetron by the

RF system. The normal operating parameters of the magnetron tube (2J56) used in this work are described below. These parameters were intentionally changed to stress the magnetron tube leading to its abnormal functioning. The effect on AE during normal and abnormal functioning of the magnetron was observed and recorded.

The normal filament voltage of the oscillator tube is 6.3 volts AC obtained through a step down transformer whose primary operates at 115 volts AC. By decreasing the voltage of the primary from 115 to 60 V, the cathode emission can be decreased to produce abnormal current pulse. This is the first deviation from the normal parameter.

The normal operating high-voltage pulse rate is 1000 pulses per second, which can be increased up to 1500 pulses per second or decreased to 100 pulses per second. This is the second deviation from the normal parameter. The pulse width is maintained constant at 1 μs. In this work, the pulse rate was changed within the range of 100 to 1000 pulses per second. With 1000 pulses per second, the average power output was around 50 W. With 100 pulses per second, it reduces to 5 W.

The ambient room temperature is about 20 ℃. With 100 pulses per second, the temperature of the magnetron rises to 35 ℃. Air from a fan cools the magnetron. A second fan keeps the waveguide load cool. The third way to stress the tube is to shut off the first fan and let the temperature of the magnetron rise. The temperature rise was rather rapid with the high pulse rate of 1000 pulses per second.

The RF energy produced by the tube is delivered to a load at the end of the waveguide. By using a variable and movable load impedance attached to the waveguide, part of the RF energy can be reflected back to the magnetron, creating an abnormal operating situation. Changing the ratio of the reverse power to the forward power is the fourth way to stress the tube. The average RF output power of the magnetron was measured with a Hewlett-Packard Model 432A power meter. Two attenuators in series (each 10 dB) were used to connect the cable of the power meter to the waveguide when the power output was around 50 W, and one attenuator was used when the power output was around 5 W.

The normal pulse voltage is 15 kV and can be increased up to 21 kV. This is the fifth way to create abnormal operating parameters. However, this deviation may produce arcing among components inside the high-power supply cabinets. For this reason, it is used sparingly in this work. It was observed generally that when the tube was stressed, it produced abnormal current, and resulting abnormal RF pulses. The abnormal current pulse is captured with the masking feature of the oscilloscope, the data acquisition is stopped, and the magnitude of the FFT is calculated for the captured AE signal from the magnetron. The frequency spectrum of AE activity is expected to be less than 1 MHz. The sampling rate used was 250 MS/s. The displays on the oscilloscope screen were saved on a computer disc in bit map mode. This procedure was repeated many times with normal and varied abnormal functioning of the magnetron tube. The AE activity was monitored by the four previously described transducers in turn. The preamplifier gain and the post-amplifier gain were monitored and kept unchanged when two oscilloscope displays were considered for comparison.

7.5 Experimental results

The data in Figure 3 were obtained by using AE transducer C (see Table 1). Figure 3 shows the masking feature and mechanism provided by the oscilloscope for capturing a signal generated

during the abnormal operation of the magnetron when it was stressed by changing one of its normal operating parameters. In both frames of Figure 3 the pulse rate was adjusted to 100 pulses per second and the oscillator filament primary voltage was set at the normal value of 115 volts. In both frames, oscilloscope channel 3 was connected to the output of the acoustic emission post- amplifier. Channel B was connected to the current sensor of the magnetron. It shows the zoom trace of the current pulse. The mask was set on channel D (zoom trace). Channel A shows the magnitude of the FFT of the acoustic emission signal from channel 3.

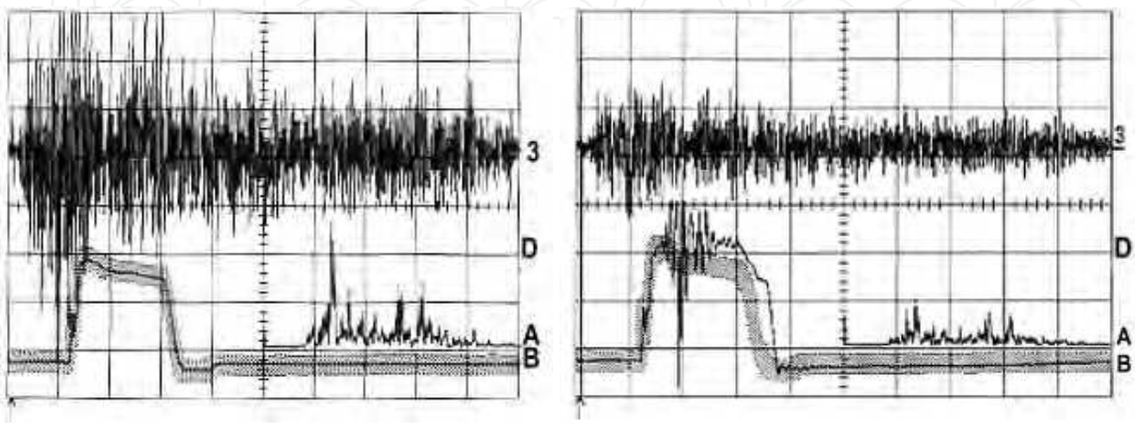

Fig. 3. Oscilloscope images of normal (pulse voltage: 15 kV) operation of the magnetron, showing AE signal on channel 3 for normal current pulse on channel B (top frame) and of abnormal (pulse voltage increased to 19.5 kV) operation showing AE signal of decreased amplitude due to abnormal current on channel B caught by masking feature (bottom frame).

In the normal operation, pulse voltage was set at the normal value of 15 kV. It then gradually increased to 19.5 kV when the abnormal current pulse occurred. When it was outside the mask value, the oscilloscope displayed the abnormal pulse. This display was then stored on the disc.

Let us compare the two acoustic emission signals. The preamplifier and the postamplifier gains were kept unchanged. In both frames of Figure 3 the vertical sensitivity on channels 3 and A were kept unchanged at 100 mV/division (millivolt/division) and 14.6 mV/division, respectively. Now compare the amplitudes of the acoustic emission signals in both frames on channel 3. When the abnormal pulse occurred, the acoustic emission signal amplitude was decreased considerably (right frame) in comparison with the one obtained during the normal operation (left frame). Also shown is the abnormal current pulse caught by the masking feature. Channel A shows the FFT of the AE signals.

Next, the data in Figure 4 were obtained using transducer A (see Table 1) coupled to the magnetron anode. The pre-amplifier gain at 20 dB and the postamplifier gain at 0 dB were held constant. The pulse rate was 1000 pulses per second and the pulse voltage was 15 kV. The pulsed microwave power of about 40 kW was sent forward to the load at the end of the waveguide and no power was reflected back. These normal parameters were held constant except for the oscillator's primary filament voltage. For the data in the left frame of Figure 4, it was set at the normal value of 115 volts, while for the data displayed in right frame of Figure 4, it was gradually decreased to the value of 95 volts when the abnormal current pulse occurred. The display from the oscilloscope screen was immediately recorded on the

floppy disc. In records of both frames in Figures 4, channel 3 was connected to the output of the AE post- amplifier. Channel B in left frame of Figure 4 shows the zoom display of the normal current pulse while in right frame of Figure 4, it shows the zoom of the abnormal current pulse.

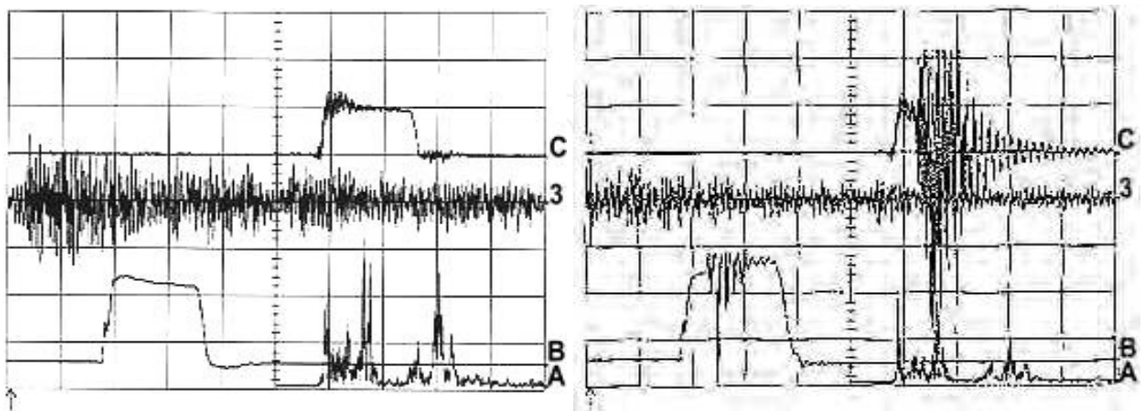

Fig. 4. Oscilloscope images of normal (filament transformer primary voltage 115 volts) operation of the magnetron, showing AE signal on channel 3 for normal current pulse on channel B (left frame) and of abnormal (filament primary voltage reduced to 95 volts) operation showing AE signal of decreased amplitude due to abnormal current on channel B (right frame). No mask is shown here. It is hidden.

Channel C in the left frame of Figure 4 shows the zoom display of the normal RF signal related to the RF power taken out from the waveguide, while in the right frame of Figure 4, it shows the zoom of the abnormal RF signal. AE signals are shown on channel 3, one of high amplitude in left frame due to normal operation and of decreased amplitude in the right frame due to abnormal operation. The magnetron was forced to behave abnormally by changing the value of the oscillator filament primary voltage. A similar decrease in AE signals was observed using different abnormal conditions such as load mismatch at waveguide, causing the power ratio (reflected power to incident power) to change. The details of different abnormal situations used and corresponding AE patterns obtained using different transducers are reported by Joshi et al. (2000, 2006 and 2007). Irrespective of the cause of the abnormal functioning, it produced a decrease in the amplitude of the burst type of AE signal. Channel A shows the FFT of the AE signals.

7.6 Discussion of magnetron experimental results

Under abnormal operation of a high-power magnetron radar tube induced by different stressing mechanisms, the AE signal consistently showed a measurable decrease in amplitude relative to the AE signal amplitude recorded during normal functioning of the tube. The phenomenon observed was independent of the AE sensors used to pick up the AE signal from the grounded cylindrical anode of the magnetron tube. The details of the mechanism of generation of acoustic emission due to the pulsating of the RF electromagnetic wave is under investigation. The pulsing electromagnetic energy generates a thermal shock wave in the cylindrical grounded anode that in turn produces the acoustic emission stress wave due to elastic properties of its material. Acoustic energy could also be generated by the interaction of

1-μs, 16-A current pulses with a strong magnetic field. The decrease in the pulsating electromagnetic energy in the abnormal functioning of the tube shows the related decrease in the energy of the acoustic emission signal. These result proved that one can use advanced AE technology for in-situ performance monitoring of radar tube like magnetron.

8. Application of AE technology to klystron high power microwave tube

8.1 Experiment on first klystron unit

The unit used in this work was a five-cavity klystron amplifier. Joshi et al. (2001, 2002, and 2007) and Ramirez et al. (2003) have published the details of the functioning of the klystron unit with auxiliary electronic circuits. The pulse repetition frequency (PRF) was chosen at 213 pulses per second. An adjacent pair of pulses was generated. The pulse width of the first pulse was 2 μs and that of the second pulse was 125 μs. The separation between two pulses was 125 μs. The RF frequency of the first pulse was 894.33 MHz. The second pulse was the chirp signal with the center frequency of 894.33 MHz and the variation of ±1/2 MHz. In other words, the chirp range was 1 MHz. The klystron had 48 channels between 851 and 942 MHz. The low band is made of channels 1 to 16. The middle band is made of channels 17 to 32. The high band is made of channels 33 to 48. The klystron was connected to the dummy load at the end of the waveguide. The dummy load was cooled by circulating water. In the normal operation, the cathode was held at -42 kV with respect to the grounded collector.

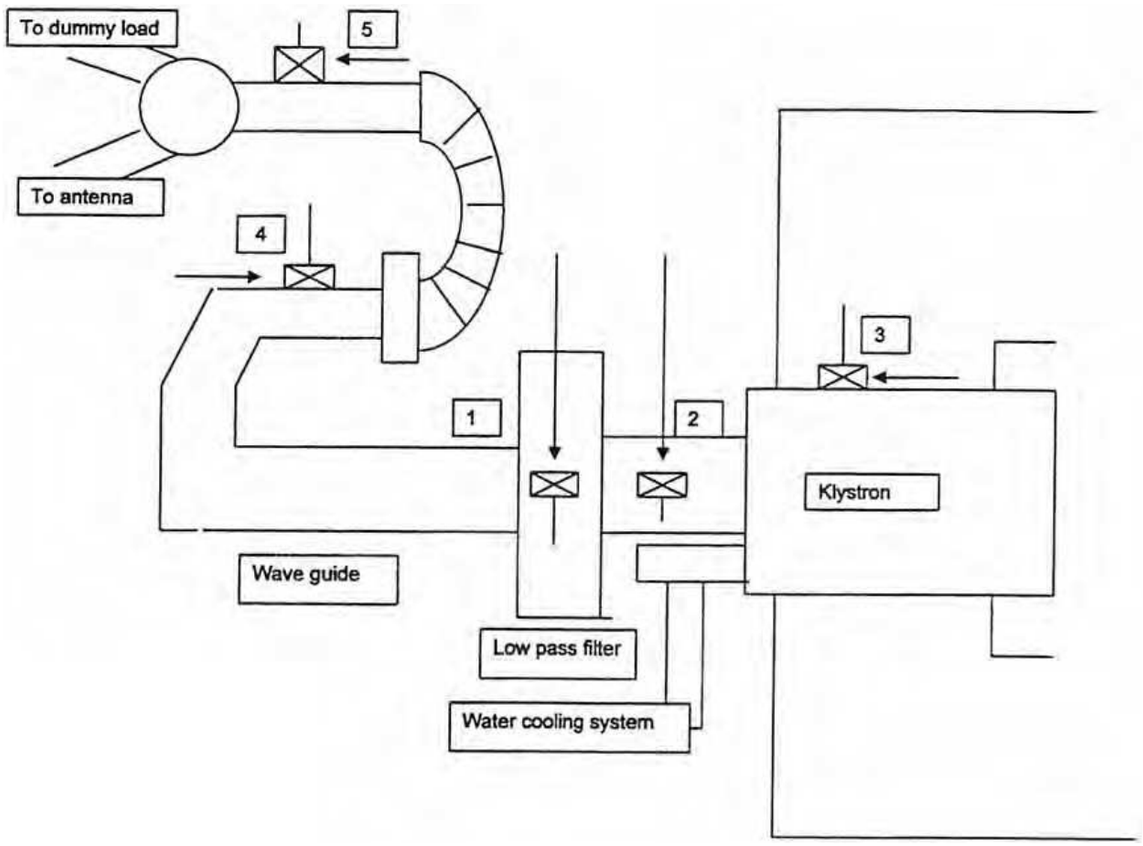

Fig. 5. Schematic of AE transducer locations on the first klystron unit.

8.2 Experimental setup

The acoustic emission system used included the general purpose transducer A (see Table 1), a preamplifier and a postamplifier as described earlier. Figure 5 shows the different locations on the klystron unit where the AE transducer was attached in turn to pick up emissions generated during the operation of the klystron. The pre-amplifier was wrapped in a bag of aluminum foil to prevent it from picking of extraneous signals. The appropriate coaxial cables (RG 223U) were used for all connections. The total gain of two amplifiers was set at 61 dB. The LeCroy 9354AM 500-MHz digital oscilloscope was used to search for abnormal acoustic emission signals generated and to store them on a disc.

8.3 Experimental results from first klystron unit

8.3.1 Effect of different locations of AE sensor

When all parameters such as gains of two AE amplifiers and transducer couplings were held constant, the strength of the AE signal differed from locations to locations during normal operating conditions of the klystron unit. The AE signals received from the location of 5 on the waveguide and from the location of 3 (Figure 5) on focusing coils inside the cabinet of the klystron unit were stronger than the one received from the location of 1 on a low pass filter.

8.3.2 Effect of increased peak power output

The klystron unit was well protected by various sensors to avoid abnormal variations of the operating parameters. The only way to stress the klystron unit was to change the peak power output, so it was decided to stress the unit by changing this single available parameter. The AE transducer was coupled to the location 3 (Figure 5) on the focusing coils of the klystron unit. In the left frame of Figure 6, four separate signals appear on the zoom trace A, which is the averaged acoustic AE signal from Channel 3. They corresponded with rise and fall of signals from beam current sensor connected to Channel 2 of the oscilloscope.

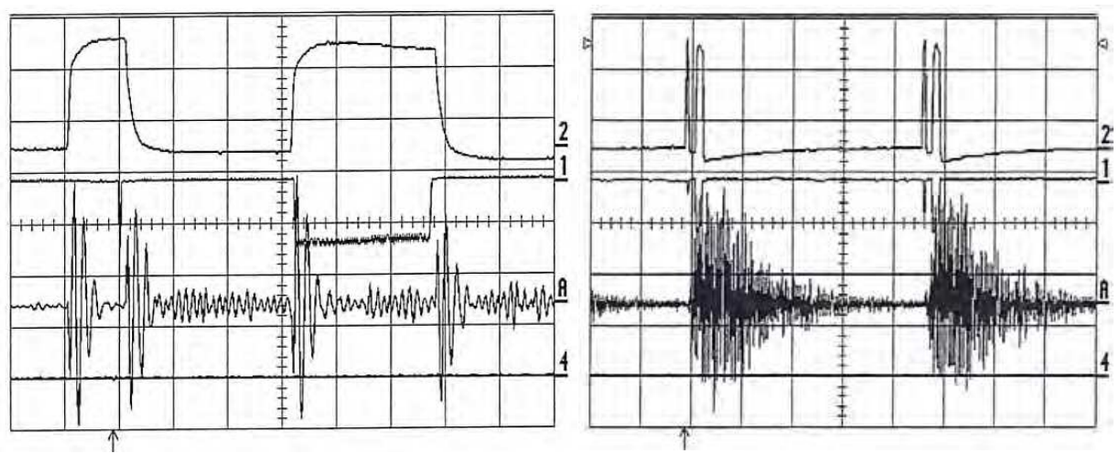

Fig. 6. Oscilloscope screen images showing signature signals from AE corresponding to one pair of beam current pulses (left frame) and two pair of beam current pulses (right frame) during normal operation.

Channel 1 shows two detected (negative 50 mV) RF drive signals. The first narrow signal 2-μs wide is around the second vertical division. The second signal, 125-μs wide and 50-mV deep, is immediately beyond fifth vertical division.

The pulse repetition rate selected was 213 pulses per second and the klystron unit was operated at a frequency of 851 MHz. In the right frame of Figure 6, the horizontal time scale was changed to 1 ms per division in order to see the next pair of pulses. The time interval between successive pair of pulses was 4.69 ms (milliseconds). Here, each pulse is a pair of pulses in rapid succession. Two pairs of beam current on channel 2 are separated by 4.7 ms (4.7 divisions x 1 ms per division). The same is true for RF drive signals (-50 mV) on channel 1. The operation of the klystron unit thus produced corresponding acoustic emission signals that appeared on channel 3. Their averaged version appears on zoom trace A in both frames of Figure 6. No AE signals appeared between the beam current pulses.

Since location 3 was giving strong AE signals, the transducer was set now set on location 4 (Figure 5). In both frames of Figure 7, channel 3 shows an AE signal. Channel 1 shows a RF drive signal and channel 2 shows a beam current sensor signal. The left frame of Figure 7 shows the normal picture when the klystron unit was operated under normal conditions. The normal operating range for the beam current was 0.9 to 1A. The peak power output was about 280 kW. To stress the klystron unit, the output power was increased by increasing the beam current slowly to the level of 1.1A, when suddenly an abnormal current pulse appeared and the threshold amplifier responded with a Transistor-Transitor Logic (TTL) high level output on channel 4 (as shown in right frame of Figure 7). The abnormal performance leads to a decrease in AE response (Channel 3) as expected. In Figure 7, vertical and horizontal sensitivities on channels 1 and 2 are the same. However, vertical sensitivity on channel 3 was 20 mV/division in the left frame of Figure 7 and was 50 mV/division in the right frame. When the vertical sensitivity on channel 3 of the right frame was changed to 20 mV/division, for comparison of two AE signals, the AE signal amplitudes in the right frame under abnormal operation would still be much smaller than the ones from the left frame of Figure 7. Thus, it was experimentally proven that the AE signal amplitudes decreased in abnormal performance of the klystron unit similar to tests on the magnetron.

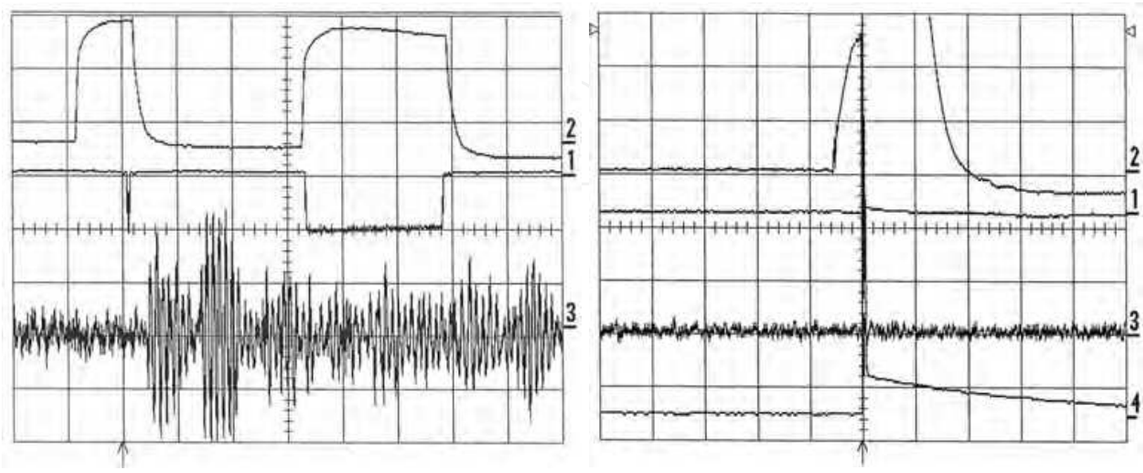

Fig. 7. AE signals on channel 3, strong during normal operation (left frame) and weak during abnormal operation (right frame).

8.4 Experiment on second klystron unit

Encouraged by the results of the acoustic emission nondestructive testing technique on the normal and abnormal operation of the first klystron unit, it was decided to repeat the experiments on the second klystron unit from a different location with different operating parameters. The second Klystron radar set had the instrumented range of 474 km (kilometers). The transmitter of the system amplifies the 2–mW (milliwatt) RF drive signal from the receiver to a 9.8- kW average power level. The amplification is performed in two stages by a driver, and the power klystron unit. The RF energy is routed to the antenna through the microwave group (coaxial cable and waveguide). The RF drive power rating was 30 W. The filament voltage requirement was 8 V. The focusing coil current required was 15 A. The frequency band called the mid-band extended from 881.333 to 910.222 MHz. The radar operates in frequency agile mode as well as in the fixed frequency mode. The fixed frequency used during this work was 902.999 MHz**.** Further details on both klystron units are available from Joshi et al. (2007).

8.4.1 Experimental setup for second klystron unit

The experimental equipment and arrangement was similar to that used with the first klystron unit (Figure 2). The radar was set into operation in the long pulse mode. The pulse repetition frequency (PRF) chosen was 254.4 Hz. The pulse repetition period was 3.93 ms. The duty cycle was 0.0377. The average RF power was 9.04 kW and average dBm (1 milliwatt reference) was 69.6. The short pulse width was 10 μs and the long pulse width was 137.5 μs. The pulse separation was 160 μs. The RF was 902.999 MHz. The RF signal was fed to a dummy load at the end of the waveguide.

8.4.2 Experimental results from second klystron unit

a. Collection of data during normal operation

Figure 8 identifies the various locations at which the AE transducer was mounted in turn to examine the AE signal patterns generated by the traveling RF pulse energy through the waveguide. To start with, the AE transducer B (see Table 1) was used to pick up AE signals. As before, the output of the transducer was connected to the input of the preamplifier set at the 40-dB gain. The output of the postamplifier set at 21-dB gain was connected to channel 3 of the oscilloscope. Channel 2 of the oscilloscope carried a T-shape BNC connector. Its one terminal was connected to klystron current (5A/V) terminal. The other terminal of the T was connected the high pass filter. The output of the high pass filter was connected to the detector. The output of the detector was connected to the low pass filter. The output of the low pass filter was connected to the threshold amplifier. The output of the threshold amplifier was connected to channel 4 of the oscilloscope. The zoom trace C was used to show the averaged AE signal from channel 3.

b. Effect on AE of different locations of AE sensor

To make sure that the equipment was not picking up extraneous signals from air, the transducer was held in air while the klystron current pulses were turned on. No AE signal was received on channel C of the oscilloscope. The AE transducer was then coupled with the viscous couplant to the top of the low pass filter at location 4. The AE signal in step with the

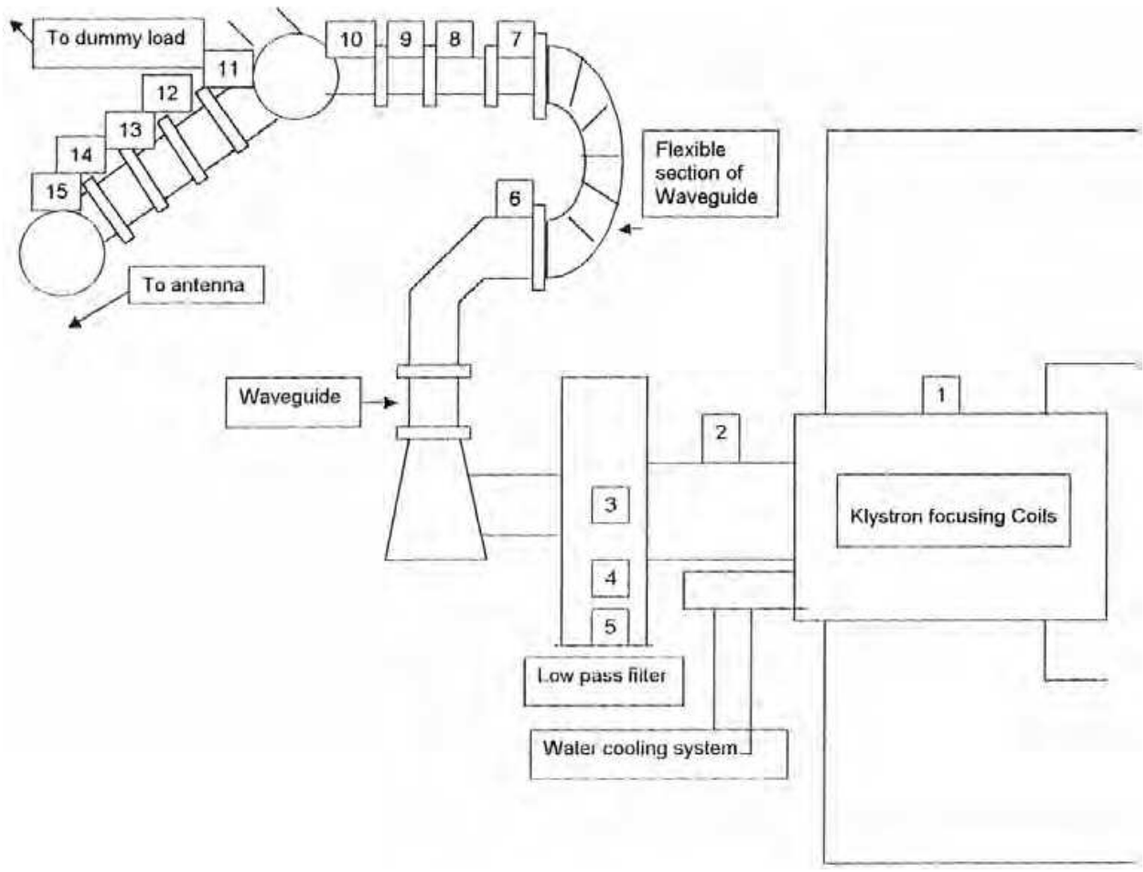

Fig. 8. Schematic of AE transducer locations on the second klystron unit.

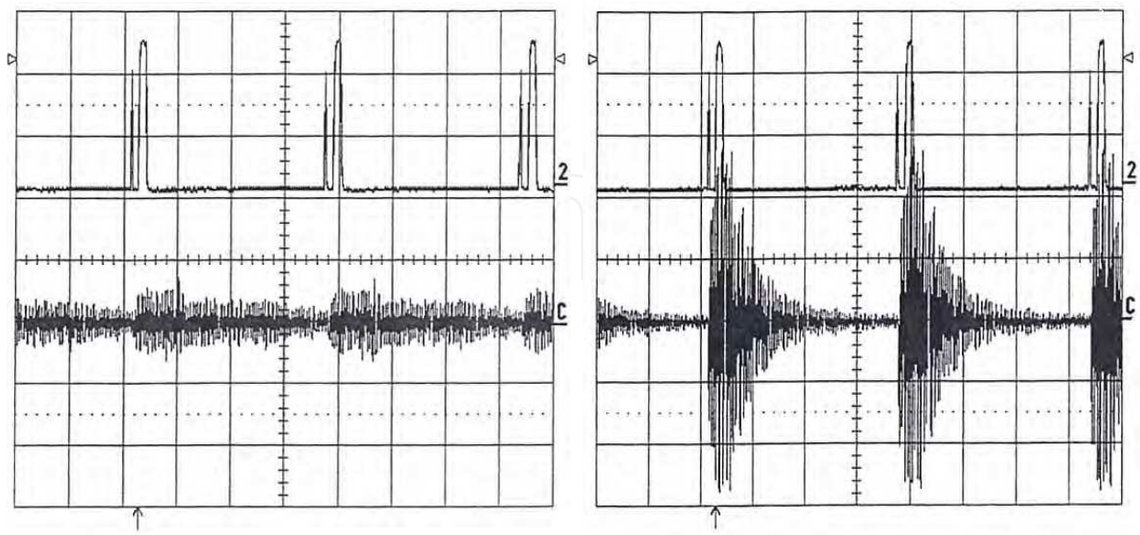

Fig. 9. AE signals in step with beam current pulses during normal operation. Signature signals from AE sensor at location 4 (left frame) and stronger signals from location 8 (right frame).

current pulses was recorded on channel C (averaged signal from channel 3) as shown in Figure 9. Channel 2 shows three pairs of the klystron beam current pulses separated by about 3.93 ms. The horizontal time scale on channel 2 was 1 ms/division. The acoustic emission activity of burst type appeared on channel C in step with beam current pulses.

The AE activity recorded was the strongest at location 8, on the isolator section of the waveguide, among all locations, as seen in the right frame of Figure 9**.** The vertical sensitivity on channel C was 50 mV/division in the left frame of Figure 9 while it was 0.50 V/division on channel C of the right frame. During collection of data from different locations on the waveguide, gains on both AE amplifiers were held constant so that AE signal data from different locations could be compared. The AE transducer was coupled properly at every new location so that no air bubbles were trapped in the couplant layer.

c. Data Collection during Stressed Operation of Klystron

The experimental setup was similar to the one used for experiment with the first klystron unit. The total gain of the AE preamplifier and the postamplifier was set at 61 dB. The AE transducer was set on the coaxial cable at the location 2 (Figure 8). The beam current was slightly less than 1 A. The AE activity was recorded during normal operation as shown in left frame of Figure 10. Channel 2 shows beam current pulses and channel C shows the averaged AE signal. Next, the high voltage was gradually increased beyond the normal value of 40 kV. The current showed a slight increase beyond 1 ampere and then the TTL output of the threshold amplifier was recorded on channel 4 as seen in the right frame of Figure 10. The recorded AE signal during abnormal operation is shown on channel 3 without being averaged. The averaging operation removes noise from the signal. The vertical sensitivity was set at 200 mV/division on channel C in the left frame (normal operation) while it was set at 50 mV/division on channel 3 in the right frame (abnormal operation). The comparison of strengths of two AE signals (200 mV/division x 4 divisions = 800 mV in the left frame while 50 mV/division x 4 divisions = 200 mV in the right frame) shows that during abnormal operation strength of AE signal decreased provided all other parameters were kept unchanged.

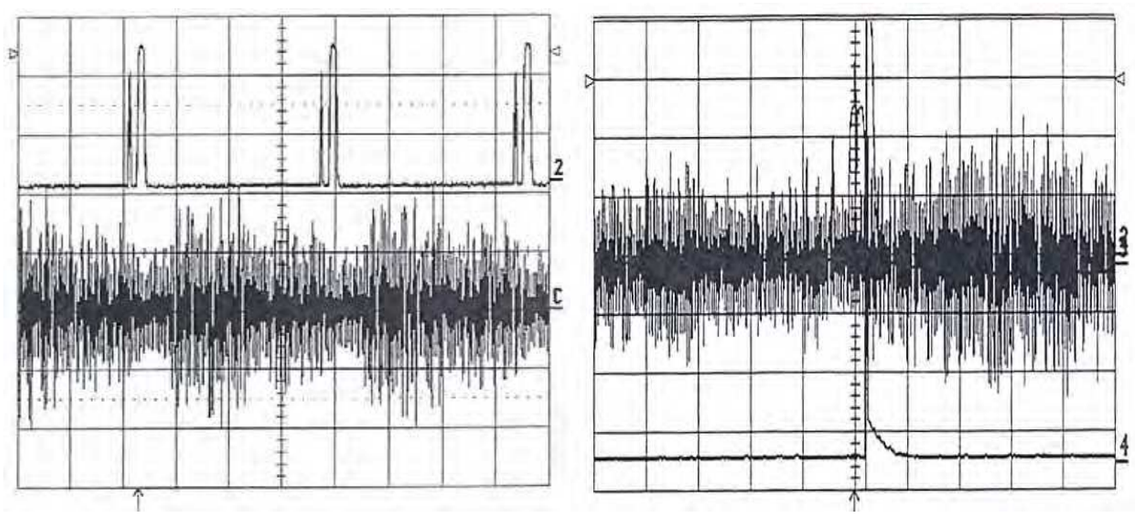

Fig. 10. Strong AE signal on channel C during normal current pulses on channel 2 (left frame) and weak signal due to abnormal current pulse on channel 2 (right frame).

In the right frame of Figure 11, the horizontal time scale was expanded to 0.5ms/division from 1ms/division so that the abnormal beam current pulse from the right frame of Figure 10 could be seen clearly. Signals from other channels were not displayed. In the right frame of Figure 11, the time scale was further expanded to 50 μs/division on the zoom trace A of channel 2 in order to see the fine structure of the abnormal pulse.

In the pair of consecutive pulses in the right frame of Figure 11, the first pulse is 10-μs wide, seen just before the first vertical line. The second pulse started just before the fourth vertical line. The separation between two consecutive pulses was 160 μs as expected. The second pulse of 137.5-μs width developed a dip in its structure as seen on the fifth vertical line. This abnormal structure in the second beam current pulse caused the threshold amplifier to trigger TTL outpu.

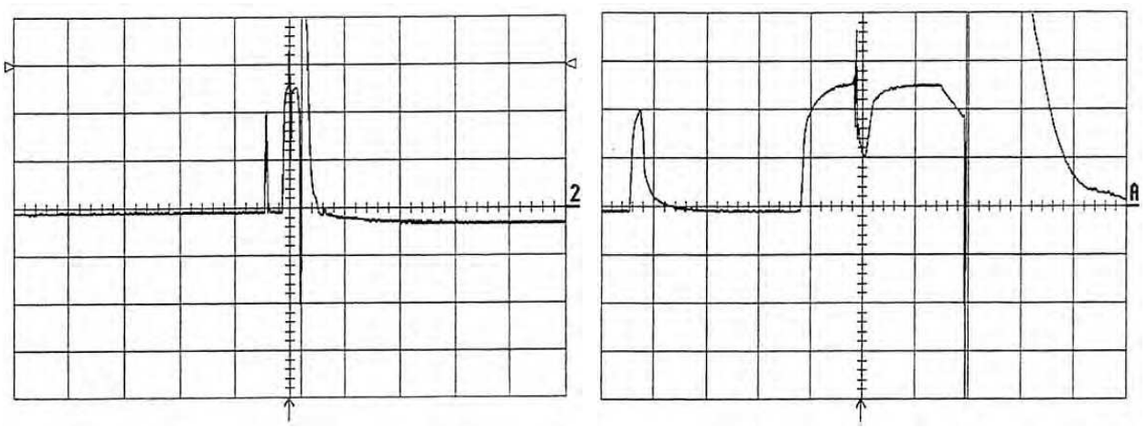

Fig. 11. Both left and right frames show expanded view of the same abnormal current pulses with horizontal time scale equal to 0.5 ms/division (left frame) and is equal to 50 μs/division.(right frame).

The normal or good pulse will not trigger the threshold amplifier output that was connected to channel 4. It takes its input from channel 2 (of the klystron beam current pulses) through the high pass filter, detector, and low pass filter. An abnormal pulse produced by stressing the klystron tube beyond its normal operating range has high-frequency components. The high pass filter (beyond 1.6 MHz) stops the regular pulse and let the abnormal pulse go through. The detector detects it and passes it to the low pass filter (below 15 MHz), which cleans up the signal. It was passed to the threshold amplifier, which responded with TTL output. Further details on the electronic circuits for detection of abnormal pulses can be obtained from Joshi et al. (2001 and 2002) and Ramirez et al. (2003).

8.4.3 Conclusions from klystron operations

The advanced nondestructive technique of acoustic emissions was applied for the first time in the current research project for in-situ performance monitoring of two high-power microwave tube klystron units. Positioning the AE transducer at different locations on the waveguides of the klystron units produced remarkably different AE patterns. The abnormal operations of tubes showed a decrease in strength of AE signals when compared with AE signals from a tube operating under normal conditions.

9. Application of AE technology to traveling wave tube

The TWT (Traveling Wave Tube) is an electron tube used for amplification at microwave frequencies. Microwave frequencies are generally identified as frequencies above 500 MHz. The operation of a TWT depends on the interaction of a beam of electrons with an electromagnetic wave. The most common traveling wave thermionic device is the linear beam TWT. Because of their very wide bandwidth, and high-power gain, traveling wave tubes are extensively used in radar, space communication, and electronic countermeasure (ECM) systems.

The high-power TWT is a microwave amplifier characterized by high gain, large bandwidth, relatively low efficiency, and high operating voltages. The electron gun assembly of a TWT consists of a filament and cathode, grid, anode, and collector. It is a tetrode tube. In addition, it has a helix structure for an RF signal to be amplified. Electrons leaving the electron gun are accelerated through the helix structure to the collector by the high voltages from the power supplies. The TWT uses a series of permanent magnets to provide a partial focus for the electron beam. The grid, anode, helix structure, and collector voltages 'fine tune' the beam focus so that a minimum of electrons strike the helix. Very few electrons strike the helix structure. An RF signal passes into a vacuum interior of the tube through a ceramic window at the RF input and then propagates through the slow-wave circuit (the helix) with a phase velocity approximately equal to the electron beam velocity. The beam and the propagating RF signal interact such that energy is transferred to the RF signal. Application of an RF signal to the input of the helix structure causes alternately accelerating and decelerating electric fields along the helix structure. Electrons passing through the helix will either speed up or slow down, depending on which part of the field they are located. Electrons that are slowed down meet with electrons that are accelerated by the preceding field. Thus, the input RF signal interacts with the electron beam, causing it to bunch up. This process grows as the beam travels through the helix and the amplitude of the RF wave associated with the bunched electrons increases. The amplified RF signal then passes out of the vacuum interior at the RF output, and the spent electron beam is absorbed by the collector. Heat energy is dissipated in the collector structure and heat sink, which are cooled by the high-efficiency air blower. The helix has a virtually constant phase velocity over a wide range of frequencies and has by far the largest bandwidth of any slow-wave structure. It possesses a high-interaction impedance and is thus able to produce a high gain in a short length.

9.1 Traveling Wave Tube Amplifier (TWT-A)

The TWT-A (Model A600/L-878A) unit used in this research work was designed and manufactured by Logimetrics. It is used to linearly amplify microwave signals over the operating bandwidth of 1 GHz (1 GHz to 2 GHz). The TWAT-A unit was self-contained. It obtained its power through 30-A/115-V thick cable from the three-prong wall socket. The intake air is filtered through a filter on the front panel. The exhaust fan is located in the rear of the unit. The front panel carried three meters, one for the collector current (range: 0 to 1 Ampere DC), one for the helix current (range: 0 to 100 mA DC), and one for power in watts (range 0 to 500 W forward and 0 to 100 W). The front panel also carried the amplifier RF gain control (a 24.5 turn potentiometer acting as a 0- to 20-dB attenuator). Five overload shutoff mechanisms protect the unit. The front panel carries five

corresponding fault indicator lamps indicating TWT-A thermal overload, power supply thermal overload, cooling air supply faults, VSWR cutoff, and helix current faults. The unit has an AC power main breaker, a power-on switch, and a two-position Standby/RF on switch. The timer inside the unit waits 3 minutes after the main circuit beaker and 'power on' switch are turned on. When the standby indicator lamp is turned on, the switch can be changed to the 'RF on' position.

The TWT-A used in this work provides in excess of 200 W of CW (continuous wave) power over the operating range of 1 to 2 GHZ. The unit is protected by helix sensing current and voltage sensing circuitry. An internal RF system detects high VSWR and automatically turns the amplifier off while simultaneously lighting up a VSWR fault lamp on the front panel. The TWT-A operates safely into an impedance mismatch that will produce a VSWR of 2.5:1. The input and output impedance were 50 ohms. The input and output connectors were N-type. The small signal region of the input/output characteristics is characterized by linear operation, low intermodulation products, and low harmonic generation. The gain of TWT-A is usually 6 to 8 dB lower at saturation than the gain available at the small signal. The gain decreases further into the overdrive region. The details are available from Logimetrics (1998).

9.2 Experimental setup

In the normal operation of the TWT-A, the output is connected to the waveguide leading to an antenna. In the laboratory, it was connected through the high-power directional coupler to a dummy load of the ratings of 50 Ω and 225 W. To remove heat, the dummy load carried a fan that could be run directly by the regular power supply. The high-power directional coupler was rated at 200 W, with a frequency range of 960 to 1215 MHz, and a coupling of 30 dB. It carried four N-type connectors J1, J2, J3, and J4. The input connector J1 was connected through the N-type coaxial cable (Alpha wire 92194-RG 214/U) to the output terminal on the rear panel of TWT-A. The output connector J2 was connected through the N-type coaxial cable to the dummy load. The forward connector J3 was connected through the N-type coaxial cable to the 20-dB attenuator in series with the 10-dB attenuator. The other end of the 10-dB attenuator was connected to the input terminal (50 Ω and 9 MHz to 22 GHz) of the HP 8562A spectrum analyzer. The two attenuators had ratings of medium power of 20 W and a frequency range of DC to 11 GHz. They carried metal fins to dissipate heat. The details of the circuit diagram can be obtained from Joshi et al. (2008).

The "T" connector between the two attenuators carried an inline crystal detector with a N-type connector on one end and a BNC connector on the other end. It is a square law crystal detector made of a silicon microwave diode. It was connected through the regular BNC cable (Pomona Electronics 2249-C-48) to Channel 2 of the LeCroy 9354AM 500-MHz digital oscilloscope. The input signal to TWT-A was generated by a HP 8352A RF plug-in module of a HP 8350B sweep oscillator. The type-N output connector from the module was connected through the type-N coaxial cable to the type-N input connector on the rear panel of TWT-A.

The right cover of the rectangular box-shaped TWT-A unit was opened. The TWT tube enclosed in the metal box was detected under the air circulation duct. The AE transducer A (see Table 1) was then mounted on the side of the TWT metal casing using the couplant

silicone compound (Mil-S-8660B, General Electric Company). It was held in position by padding of foam inserted between the back of the transducer and the frame of the TWT-A unit. The transducer is then connected to the pre-amplifier. The pre-amplifier output was connected to the post-amplifier. The output of the main amplifier is connected to channel 3 of the LeCroy digital oscilloscope. The sampling rate of the oscilloscope for single channel was 2 Gs/s with 1 million points. If four channels are used at the same time, the sampling rate would be 500 Ms/s with 250 kilopoints per channel**.**

9.3 Experimental procedure

The maximum input power recommended for the spectrum analyzer is 0 dBm (1 milliwatt reference). The input power from the 83525A RF plug-in can be changed in steps. The frequency of the CW input signal was initially chosen to be 1.2 GHz. The output of the TWT-A unit was connected to a 50-Ω dummy load through the high- power directional coupler. The RF gain control knob (20-dB attenuator) from the front panel was set all the way in the clockwise position, indicating that the selected full input power is applied to TWT-A for amplification. The front panel power indicator had two scales, one for the forward power in the up position of the switch and the second for the reverse power in the down position of the switch. This power was attenuated by 60 dB (30-dB directional coupler + 20-dB attenuator +10-dB attenuator) before it was fed to the input terminal of the spectrum analyzer.

9.4 Experiments and results

The purpose of this research project was to check the feasibility of using acoustic emission as the noninvasive tool to monitor performance changes in the TWA-A. Such application of AE technology for in-situ performance monitoring of high-power microwave radar tubes of a pulsed magnetron and a klystron unit were demonstrated successfully in the earlier part of this chapter. In the earlier experiments on two radar tubes of pulsed magnetron and klystron, the radar units made it easy to introduce variations in the normal working parameters of the tubes, thereby producing abnormal pulsed outputs. AE transducers immediately indicated differences between normal and abnormal functioning of tubes. In the case of TWT-A, the unit was protected with five sensors. Thus, the tube did not allow much variation in the normal working parameters. It was decided therefore to use the TWT-A unit in two different modes (CW mode and pulsed mode) and check the ability of acoustic emission to detect the difference.

9.5 Part I -CW mode with dummy load of 50 ohms

Here, the aim was to observe acoustic emission activity under the normal operation of TWT-A in CW mode when the output was connected to the 50-Ω dummy load through the 30-dB directional coupler. An AE transducer was mounted on the TWT near the output terminal of the helix. The normal noise band on channel 3 was covered with the mask (zoom trace D) of a height sufficient to avoid triggering on the noise signal. The trigger level was chosen slightly below the upper boundary of the mask. The trigger position was set at two divisions to the right of zero on the horizontal scale. If all the points of the signal remain within the mask, there will be no beep sound and no automatic dumping of the screen display on the

3.5-inch floppy disc in the disc drive of the oscilloscope. The arrangement ensured recording of the AE burst signals only, avoiding noise signals. To avoid damage to the oscilloscope screen, the mask on the zoom trace D is set and then turned off during prolonged operation of the equipment. Nine AE events were recorded on the disc in 3 hours. Changes in the detected RF level on channel 2 were expected, assuming that AE signals were produced due to the irregular functioning of TWT-A. In the left frame of Figure 12, the horizontal scale was set at 0.1 ms per division on channels 2 and 3. The vertical sensitivities were 10 mV per division on channel 2 and 50 mV per division on channel 3. Figure 12 (left frame) shows the typical AE signal on channel 3 and the detected RF level on channel 2 at -22 mV. No appreciable changes were detected in the AE signal or in RF level during the 3 hours. The sporadic presence of AE signals could be taken as an instantaneous variation in the normal parameters of the unit. Since the unit was protected by five sensors, the system gets restored instantaneously.

9.6 Part II (CW mode with no load-all power reflected back).

9.6.1 Effect of closing the front air inlet

It was then decided to stress the TWT-A operation by forcing it to operate at higher temperatures, which in turn could produce irregular RF amplified pulses and corresponding changes in AE signals. The front-panel air inlet was covered tight with aluminum foil sealed around the edges. The dummy load was disconnected and was replaced by a teflon (insulator) plug between the central pin and the surrounding metal cylinder of the N-type connector. This was done to reflect the RF power in order to stress the tube. Although AE signals were received at intervals, TWT-A got shut off within 8 hours due to thermal overload. The detected RF level on channel 2 did not change. No changes were detected in AE signals on channel 3 while operating the tube at a higher temperature. At this stage, the left-side and the top-side panels of the unit were opened. The five sensors protecting the unit were identified as a thermal sensor, an air flow sensor, a power supply sensor, a VSWR overload sensor, and a helix current sensor.

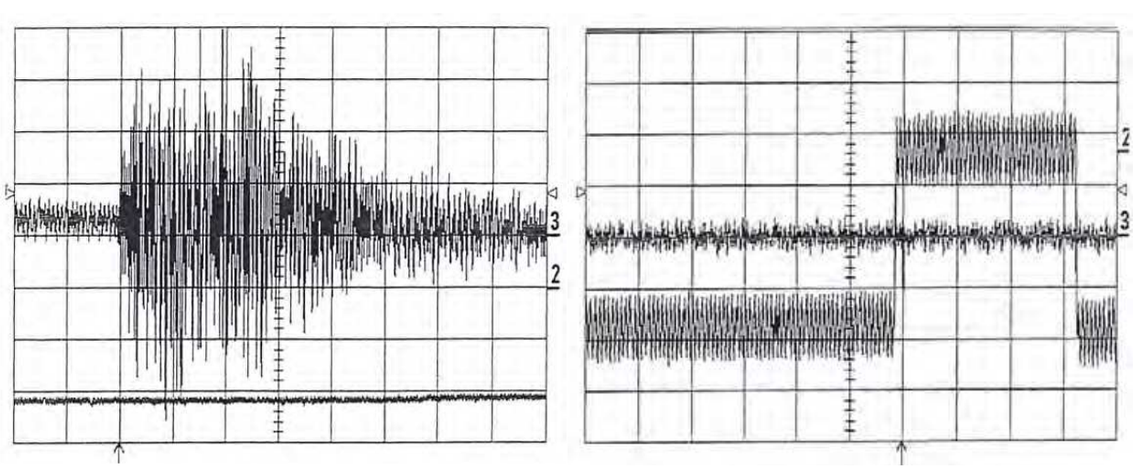

Fig. 12. Sporadic AE signal from the TWT-A in CW operation (left frame) and periodic AE signal on the sixth vertical division (compressed) from pulsing the TWT-A (right frame).

9.6.2 Effect of the different locations of the AE sensor

There was a need to find out whether the position of the AE transducer could make a difference in receiving the AE signals. For this purpose, the transducer was mounted on the metal coaxial cable running from helix output terminal to the output terminal on the rear panel. The new position of the transducer made no difference in recording AE activity. The AE activity was sporadic on and off, appearing intermittently as in the left frame of Figure 12. Next, it was decided to feed the pulsing RF input signal to TWT-A in place of the CW signal and observe the AE signatures.

9.7 Part III (Pulse mode with no load-all power reflected back)

The RF input frequency was chosen at 1.4770 GHz. The frequency span (Δf) was set on zero. The sweep trigger was on the line. The 'RF on' time was set at 2 seconds. The 'RF off' time was fixed internally at about 1 second. On the spectrum analyzer screen, the start frequency was 1 GHz at the left end. The stop frequency was 2 GHz at the right end of the screen. The resolution bandwidth was 300 kHz. The video bandwidth was 300 kHz. The sweep time was 50 ms. The input power is set 13.5 dBm on the RF plug-in. The ALC (automatic level control) mode was internal. The TWT-A was turned on. After a few minutes, the power meter on the front panel was showing a rise and fall in the output power in sync with the rise and fall of the RF signal on the spectrum analyzer screen. It was observed that the maximum power output was changing with the change of the input frequency. The gradual change in the input frequency showed that the output power peaked around 1.5040 GHz. The output power at this frequency rose to the level of 140 W. The AE transducer was mounted on the TWT-A tube near the helix output terminal. The gains of both amplifiers were kept constant. It was then observed that AE signals were generated in step with the oscillating output power of the TWT-A. They are not sporadic as before. The oscillating RF power might be producing induction heating. The subsequent contraction during the cooling period was possibly the cause of the generated acoustic emission energy. Figure 12 (right frame) shows the generation of AE signal on channel 3 at the stop of the detected 'RF on' segment and at the start of the 'RF off 'segment on channel 2. The AE signal appears to be a very narrow vertical line close to the sixth vertical division due to the choice of horizontal time scale equal to 0.2 second per division suited to show 'RF on' and 'RF off' segments, which are actually inverted in the figure. The vertical sensitivities were 10 mV per division on channel 2 and 50 mV per division on channel 3.

9.7.1 Effect of RF input duty cycle on the AE activity

Next, the effect of duty cycle on the generation of AE signals was examined. The 'RF on' interval was increased from 2 to 20 seconds at steps of 1 second. The 'RF off' interval was fixed internally at about 1 second. In every instance, the AE activity was observed to be in step with the changing RF output. Then the 'RF on' interval was reduced to 1 second, almost equal to the 'RF off' interval. The AE signals were still generated in step with changing RF output. The 'RF on' interval was further reduced to less than 1 second and AE activity started diminishing rapidly with further decrease in the 'RF on' time. It appears that the 'RF on' interval has to be greater than 'RF off' interval to generate the AE activity. It was decided, therefore, to set the 'RF on' interval at 2 seconds for future testing. Figure 13 (left frame) shows the AE signals generated with the pulse rate of 20 pulses per minute. In Figure 13 (right frame), the detected RF level is in the process of changing its value from that in left

frame. For each pulse, the 'RF on' interval was 2 seconds and the 'RF off' interval was 1 second. In both figures, the horizontal time scale was set at 0.5 ms per division on channels 2 and 3, and the vertical sensitivities were 10 mV per division on channel 2 and 50 mV per division on channel 3. In the left frame of Figure 13, the zoom trace B of channel 2 shows moving detected RF voltage at a negative 22 mV level. In the right frame of Figure 13, the detected RF level is in the process of changing its value from that in the left frame. The AE signal on channel 3 in both frames of Figure 13 appear well expanded relative to the single vertical line that appears in the right frame of Figure 12. All power was reflected back since the dummy load was replaced with the teflon plug.

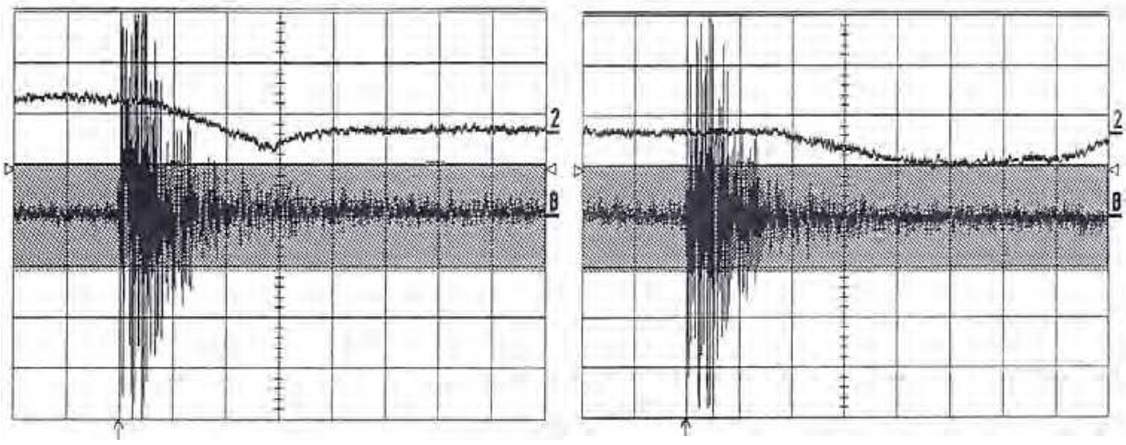

Fig. 13. Expanded view of signal from right frame of Figure 12.

To determine the 'RF off' interval precisely, the horizontal time scale was changed next, the screen displays were captured saved on the disc. In Figure 14, the horizontal time scale of 0.1 second/division was used. It was observed that the 'RF off' interval was 0.7 second (channel 2), slightly less than the assumed value of 1 second. The 'RF off' interval is internally fixed and hence cannot be changed. The AE signal from channel 3 is seen on the second vertical line in the left frame of Figure 14. Its expanded view was shown in the right frame.

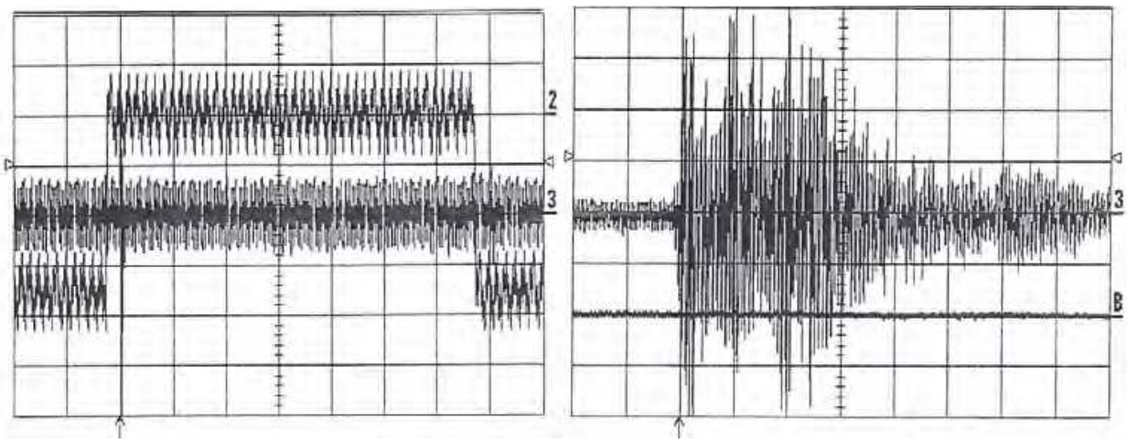

Fig. 14. Compressed AE signal (left frame) on the second vertical division in sync with the pulsating traveling wave tube amplifier and its expanded view in the right frame showing the expanded AE signal.

9.7.2 Effect of sudden 'cut off' of filament power on performance of TWT-A

The purpose of this experiment was to check the feasibility of application of advanced AE technology to detect abnormal functioning of TWT-A. Since the TWT-A unit used in the project was protected by five overload detection sensors, one has to use novel ways to induce the irregular performance of the unit. The power of the cathode/heater assembly suddenly and see its effect on the performance of the tube. Since the cathode/heater assembly was at a negative high voltage of about 2000 V with respect to the collector, the necessary high-voltage protection device was used during the sudden disconnection of the power supply to the filament. As the tube cooled off rapidly, many AE signals were generated in succession in about 1 minute before all the acoustic emissions stopped with the power output dropping rapidly from 140 W (forward power) to 0 W. It takes 15 seconds for the oscilloscope to store the screen display on its disc. It was impossible to save the AE signals on the floppy disc generated during the rapid cool-off period. However, a couple of screen displays were stored automatically during the cool-off period**.** The AE signals obtained during the simulated cold cathode experiment had relatively small amplitudes and longer ringing time.

9.7.3 Effect of cold start

The standby time between the 'power on' position of the switch and 'RF on' position is 3 minutes. The standby time was measured by closing both the air inlet and outlet windows. The times were about the same. Again, to produce some kind of irregularity in the functioning of the unit, the timing circuit governing the standby interval was bypassed by changes in the circuitry. The RF power input was set at 13.5 dBm, as before. The RF input power was pulsating with a 'RF on' interval of 2 seconds. No load was connected and all the power was reflected back. The main circuit beaker switch, the power-on switch, and the 'RF on' switch were turned on in succession to produce a cold start condition. The tube was not damaged. The only observable effect of the cold start was a little delay in receiving AE signals in step with pulsating RF power. The AE signals generated in the beginning were not strong. After about 10 minutes, strong AE signals started appearing in step with the pulsating input power and out powers.

9.8 PART IV (Pulse mode with dummy load of 50 Ohms)

The dummy load of 50 Ω was connected to the output cable. Then the RF input to TWT-A was set on CW mode as in the Part I experiment. The RF input power was 13.5 dBm. The gain setting was in the fully clockwise position, giving the maximum gain. There was no AE activity even after half an hour. Then, RF input was changed from the CW mode to the pulsating mode. The dummy load remained connected. Within a few minutes, AE signals were received just like in Figure 14. They were generated in step with pulsating RF output.

9.9 TWT amplifier operation conclusions

The CW mode operation did not produce AE activity when the output cable of the TWT-A unit was connected to the dummy load of 50 Ω (matched load), and when it was connected to the teflon plug (mismatched load), causing power to be reflected back. The pulsing RF input power generated the AE activity irrespective of the termination

(matched or mismatched load) of the output cable. The AE activity is generated as long as the 'RF on' interval in the pulsing RF input power remains longer than the 'RF off' interval. Acoustic emission signals are generated at the end of 'RF on' interval and at the beginning of the 'RF off' interval of the output RF pulse. The cold start experiment showed that the strength of AE signals was low in the beginning but they picked up the intensity after the unit was in operation about 10 minutes with pulsating input power. The simulated cold cathode experiment showed that rapid changes in the filament power supply caused AE activity in succession and stopped with the diminishing power output. Overheating, the unit did not produce any new effects since the unit was protected by the thermal overload sensor. The maximum leveled output from the 83525A RF plug-in of the 8350B sweep oscillator was 17.5 dBm. However, the unit got shut off by the VSWR overload sensor when the input power exceeded 14 dBm.

The TWT-A used in this project was meant for CW mode operation. By operating it in the pulse mode, the AE activity was produced in step with the changing RF input power. During the operation in CW mode, it was observed that whenever there was change (increase or decrease) in the RF input power, AE activity was generated. In short, changes in the RF output power, either due to irregular changes or regular changes in the RF input power, caused the AE signals to appear. These experimental observations definitely indicate that AE activity will be produced whenever the RF output power of the unit changes, irrespective of the cause of the change external to the unit (RF input power) or internal to the unit (degradation of the tube performance). The results of this work show that acoustic emission technology can be used as the nondestructive testing tool for in-situ performance monitoring of normal and abnormal functioning of high-power microwave TWT amplifiers.

10. Overall conclusions

Advanced acoustic emission technology offers a simple and direct NDT technique for real-time monitoring of in-situ performance of high-power microwave devices such as the magnetron, klystron, and traveling wave tube. The technique has proven itself as a great advancement over the currently available data collection systems using as many as 11 electrical sensors measuring different current and voltages of tubes.

11.Acknowledgment

This research work was supported by American Society for Engineering Education (ASEE) and SPAWAR Systems Center San Diego.

12. References

ASNT Handbook on "Acoustic Emission Testing" Vol. 5, 1987.

Green Robert E., "Elastic Wave Analysis of Acoustic Emission "Mechanics of Nondestructive Testing, Editor: Stinchcomb W.W., Plenum, New York, 1980. pp55-76.

Leybovich Alexander and Ferdinand R. Mark, "Sputtering Target Arc Detection Using Acoustic Emission, "Materials Evaluation, Nov. 2001, pp. 1331-1335.

Sakoda T., Nieda H., and Ando K., "Characteristics of elastic waves caused by corona discharges in an oil-immersed pole transformers," IEEE Transactions on Dielectric and Electrical Insulation, vol.8,No. 2, April 2001, pp.276-283.

Boczar Tomasz, "Identification of Fundamental Forms of Partial Discharges Based on the Results of Frequency Analysis of Their Acoustic Emission," Journal of Acoustic Emission, Vol.17, 1999, pp.S7-S12.

Boczar Tomasz, "Results of frequency analysis of AE pulses generated by corona discharges," Technical University of Opole Poland, 2001 http://cmspro.fme.vutbr.cz/uk/odbory/vav/AE2001/contrib/boczar1.htm2001.

Vahaviolos S. J., and Saifi Mansoor, "Laser Spot Welding and Real-time Evaluation," IEEE Journal of Quantum Electronics, Vol. QE-12, No.2, 1976,p.870.

Tsukamoto O., and Iwasa Y., "Acoustic Emission diagnostic & monitoring techniques for superconducting magnets," Advanced Cryogenic Engineering, Vol.31, 1986, pp.259-268.

Theobald P., Rokowski R.T., Yan T., Jarvis D., Dowson S., and Jones B.E, "Reference Source for Calibration of Acoustic Emission Measurement," IEEE Instrumentation and Measurement, Technology Conference, Budapest, Hungary, May 21-23, 2001, pp.412-416.

Edwards T.C., "Introduction to Microwave Electronics," Publisher: Edward Arnold, 1984, p.32.

Connor F.R., "Wave Transmission," Publisher: Edward Arnold, 1972, p.7.

Love Wayne, "Magnetrons," Handbook of Microwave Technology, Volume 2, (Applications), Edited by T. Koryu Ishii, Academic Press, 1995, p.36.

Watson W.H. and Troy J.W., "Computer-controlled Performance Monitor for Microwave Tubes" NOSC Technical Document 1070, Naval Ocean Systems Center San Diego, CA 92152-5000, March 1987.

Joshi, N. R., Brock, D.W., Russell S.D., Kasa, S.D., and Garcia, G.A., "Acoustic Emission Technology for Radar Tubes," Technical Note 1810, published in August 2000 by SPAWAR Systems Center, San Diego (SSC-SD), California, pages 190.

Joshi, N.R., Russell, S.D., Ramirez, A.D., and Brock, D.W., "In-situ Performance Monitoring of High Power Microwave Tubes with Acoustic Emission," published in the paper summaries of ASNT Fall Conference in Houston, 23-27 October 2006, pp.7-11.

Joshi, N.R., Russell Stephen D., Ramirez Ayax D., Brock David W., and Lasher Markham E., "Acoustic Emission Technology for Performance Monitoring of High Power Microwave Tubes," Material Evaluation, Vol.65,No.4, April 2007, pp.411-416.

Joshi, N. R., Brock, D.W., Russell S.D., Lasher, M.E., and Kasa, S.D., "Built-in Test for High-Power Microwave Tubes Using Acoustic Emission Technology," Technical Note 1816, published in September 2001 by SPAWAR Systems Center, San Diego (SSC-SD), Ca 92152-5001, pages 99.

Joshi, N.R., Russell S. D., Ramirez A. D., and Brock D. W. "Monitoring of High-Power Microwave Tube Systems Using the Integrated Condition Assessment System (ICAS)," Technical Report 1885 published in July 2002 by SPAWAR Systems Center, San Diego (SSC-SD), Ca 92152-5001, pages 116 (53+A63).

Ramirez, A.D., Russell, S.D., Brock, D.W., and Joshi, N.R., "Automated Classification of Microwave Transmitter Failures Using Virtual Sensors, " published in the

Proceedings of 13th International Ship Control Systems Symposium, 7-9 April 2003, Orlando, Florida, USA, pages 10.

Joshi, N.R., Russell, S.D., Ramirez A.D., and Brock D.W., "Performance Monitoring of High Power Microwave Radar Klystron Units with Acoustic Emission Technology," Materials Evaluation, Vol.10, October 2007, pp.1048-1053.

Logimetrics. Traveling Wave Tube Amplifier (TWT-A), Technical Manual, Model A600/L878A, 50 Orville Drive, Bohemia, NY 11716, 1998 and TWT and TWTA Handbook, Hughes Aircraft Company, Electron Dynamics Division, P.O.BOX 299, Torrance, CA 90509-2999.

Joshi N.R., Russell S.D., Ramirez A.D., and Brock D.W., "Acoustic Emission as Noninvasive Tool for Performance Monitoring of High Power Microwave Radar Traveling Wave Tube," Materials Evaluation, Vol.66, No. 4, April 2008, pp.413-418.

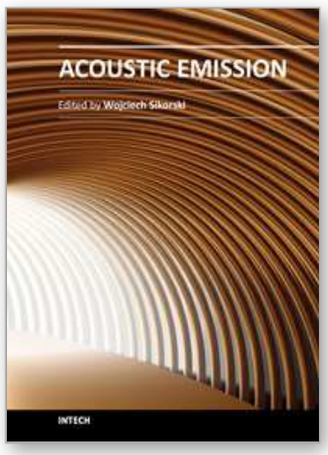

Acoustic Emission

Edited by Dr. Wojciech Sikorski

ISBN 978-953-51-0056-0
Hard cover, 398 pages
Publisher InTech
Published online 02, March, 2012
Published in print edition March, 2012

Acoustic emission (AE) is one of the most important non-destructive testing (NDT) methods for materials, constructions and machines. Acoustic emission is defined as the transient elastic energy that is spontaneously released when materials undergo deformation, fracture, or both. This interdisciplinary book consists of 17 chapters, which widely discuss the most important applications of AE method as machinery and civil structures condition assessment, fatigue and fracture materials research, detection of material defects and deformations, diagnostics of cutting tools and machine cutting process, monitoring of stress and ageing in materials, research, chemical reactions and phase transitions research, and earthquake prediction.

How to reference

In order to correctly reference this scholarly work, feel free to copy and paste the following:

Narayan R. Joshi, Stephen D. Russell, Ayax D. Ramirez and David W. Brock (2012). Advanced AE Technology for High-Power Microwave Radar Tubes, Acoustic Emission, Dr. Wojciech Sikorski (Ed.), ISBN: 978-953-51-0056-0, InTech, Available from: http://www.intechopen.com/books/acoustic-emission/advanced-ae-technology-for-high-power-microwave-radar-tubes

INTECH
open science | open minds

InTech Europe
University Campus STeP Ri
Slavka Krautzeka 83/A
51000 Rijeka, Croatia
Phone: +385 (51) 770 447
Fax: +385 (51) 686 166
www.intechopen.com

InTech China
Unit 405, Office Block, Hotel Equatorial Shanghai
No.65, Yan An Road (West), Shanghai, 200040, China
中国上海市延安西路65号上海国际贵都大饭店办公楼405单元
Phone: +86-21-62489820
Fax: +86-21-62489821

IntechOpen